Research Square

Preprints are preliminary reports that have not undergone peer review.
They should not be considered conclusive, used to inform clinical practice,
or referenced by the media as validated information.

Spatiotemporal characterization of heat waves in the semiarid region of Pernambuco, Brazil

Isabela Patrícia Andrade Figueira

isabela.andrade@ufrpe.br

Universidade Federal Rural de Pernambuco (UFRPE)

Alan Cezar Bezerra

Universidade Federal Rural de Pernambuco (UFRPE)

Alexandre Hugo Cezar Barros

Embrapa Solos

Jhon Lennon Bezerra Silva

Instituto Federal Goiano (IF Goiano)

Marcus Metri Corrêa

Universidade Federal Rural de Pernambuco (UFRPE)

Aldo Torres Sales

Universidade Federal de Pernambuco

Research Article

Keywords: Land surface temperature, Reanalysis, Climate extremes, ERA5, Environmental vulnerability

Posted Date: November 16th, 2026

DOI: https://doi.org/10.21203/rs.3.rs-11586823/v1

License: This work is licensed under a Creative Commons Attribution 4.0 International License.
Read Full License

Additional Declarations: No competing interests reported.

Spatiotemporal characterization of heat waves in the semiarid region of Pernambuco, Brazil

Isabela Patrícia de Andrade Figueira[1*], Alan Cezar Bezerra[1], Alexandre Hugo Cezar Barros[2], Jhon Lennon Bezerra da Silva[3], Marcus Metri Corrêa[1], Aldo Torres Sales[1,4]

[1] Universidade Federal Rural de Pernambuco (UFRPE), Recife, Pernambuco, Brazil

[2] Embrapa Solos, Recife, Pernambuco, Brazil

[3] Instituto Federal Goiano (IF Goiano), Campus Ceres, Ceres, Goiás, Brazil

[4] Universidade Federal de Pernambuco (UFPE), Centro Acadêmico do Agreste, Caruaru, Pernambuco, Brazil

***Corresponding author:** Isabela Patrícia de Andrade Figueira, isabela.andrade@ufrpe.br

ORCID

Isabela Patrícia de Andrade Figueira: https://orcid.org/0009-0009-6244-8453

Alan Cezar Bezerra: https://orcid.org/0000-0002-9986-9464

Alexandre Hugo Cezar Barros: https://orcid.org/0000-0002-7974-4402

Jhon Lennon Bezerra da Silva: https://orcid.org/0000-0002-2611-4036

Marcus Metri Corrêa: https://orcid.org/0000-0002-9506-8969

Aldo Torres Sales: https://orcid.org/0000-0001-6443-1884

Abstract

Heat waves are intensifying globally, particularly in semiarid regions, where the interaction between water deficit and warming amplifies thermal extremes. This study analyzed the spatio-temporal variability of heat waves in the semiarid region of Pernambuco, Brazil, from 1994 to 2023 by integrating land surface temperature (LST) derived from Landsat imagery with 2 m air temperature (Tair) from the fifth-generation atmospheric reanalysis of the European Centre for Medium-Range Weather Forecasts (ERA5). Atmospheric, surface, and coupled events were detected with a relative threshold (90th percentile) and characterized by frequency, duration, and magnitude; trends were assessed with the Mann–Kendall test. Landsat LST showed greater variability and more extreme values (maxima above 47 °C) than ERA5 Tair (maxima near 40 °C). Atmospheric heat waves showed no significant trend over the period, whereas surface heat waves became markedly more frequent, with more than 100 events per year and a significant increase in duration. Coupled events also increased, at rates above 70 events per year. Event frequency was highest in the Sertão, while the greatest magnitude intensification occurred in the transition areas of the semiarid region. Surface heat waves were more persistent (mean duration of 12 days) and carried a higher thermal load than atmospheric events (mean duration of 6 days). These results suggest that surface processes dominate the thermal stress signal in the semiarid region of Pernambuco and that air temperature alone underestimates it. Combining satellite data with climate reanalysis gave a spatially more detailed picture of thermal extremes in semiarid regions.

Keywords Land surface temperature · Reanalysis · Climate extremes · ERA5 · Environmental vulnerability

1 Introduction

Climate change has intensified extreme events, particularly heat waves, which have consistently increased in frequency, duration, and intensity globally (Mora et al. 2018; IPCC 2023). This process occurs alongside intensifying, multi-year, rapidly evolving droughts, associated with higher atmospheric evaporative demand in a warmer climate (Chen et al. 2025). The interaction between extreme heat and water deficit constitutes a compound climate hazard that amplifies impacts on ecosystems and production systems (Vicente-Serrano et al. 2022).

In Brazil, the number of days under heat wave conditions has increased in recent decades. However, limitations remain in characterizing their intensity, duration, and spatial variability, particularly at the regional scale (INPE 2023). This limitation is particularly severe in the Northeastern Semiarid region, whose vulnerability to climate change is linked to high incident solar radiation, high rainfall variability, high potential evapotranspiration rates, and the structural dependence on rainfed agricultural and livestock activities (Marengo et al. 2020; IPCC 2023; Barbosa 2024; Marengo et al. 2026). In this context, heat waves intensify water deficits by raising atmospheric evaporative demand relative to soil water availability, compromising both agricultural productivity and the functional stability of native vegetation (Barbosa et al. 2015; Miralles et al. 2019; Cohen et al. 2020).

Bartusek et al. (2022) showed that soil–atmosphere coupling amplified the 2021 heat-wave in the drylands of North America: under low soil moisture, reduced latent heat flux favors increased sensible heat flux, raising surface temperatures and amplifying thermal events. In addition, persistent atmospheric patterns, such as blocking systems, prolong these events and intensify their impacts (Jiménez-Esteve and Domeisen 2022; Barriopedro et al. 2023).

Heat waves are typically defined based on air temperatures measured at meteorological stations (Agathangelidis et al. 2022; Pant et al. 2025); however, these stations are unevenly distributed and often insufficient to represent the temperature field, particularly in arid and semiarid regions of developing countries. This limitation has been addressed using satellite data and data fusion techniques to obtain continuous temperature fields (Agathangelidis et al. 2022; Carrión et al. 2021; Schween et al. 2020).

Combinations of climate reanalysis and satellite remote sensing data have been used to characterize thermal extremes (Miralles et al. 2019; Hu et al. 2023; Silva et al. 2025). This study combines the ERA5 reanalysis, produced by the Copernicus Climate Change Service, with data from the Landsat program. With over four decades of continuous operation, Landsat provides temporal robustness to the analyses, enabling the identification of event occurrence and persistence. Meanwhile, Land Surface Temperature (LST), derived from satellite sensors with global coverage and, in the case of Landsat, high spatial resolution, allows the representation of the spatial heterogeneity in warming and captures the differentiated thermal response of the surface as a function of land cover and land use types (Barbosa et al. 2015; Jardim et al. 2022; Barbosa 2023).

Nevertheless, studies that integrate long time series of satellite data (such as Landsat) and climate reanalyses (such as ERA5) for the characterization of heat waves in the Brazilian Semiarid region are still scarce, which limits the understanding of the regional patterns of these events (Reis et al. 2019; Jardim et al. 2022).

This study hypothesizes that heat waves in the Pernambuco semiarid region have increased in frequency, duration, and magnitude in recent decades, and that their intensity is amplified by soil–atmosphere coupling and underestimated when analyzed based solely on air temperature data.

Thus, this study aimed to analyze the spatio-temporal variability of heat waves in the Pernambuco semiarid region, Brazil, by integrating satellite remote sensing data and climate reanalysis for the period from 1994 to 2023 to characterize the frequency, duration, intensity, and spatial distribution of these events.

2 Materials and methods

2.1 Study area

The study area corresponds to the Semiarid region of the state of Pernambuco (Fig. 1), as officially delimited by SUDENE (2017), located between the latitudes 7°15′S and 9°30′S and longitudes 34°50′W and 41°20′W. Within the state, the Semiarid region covers 86,341 km², including, in whole or in part, 123 municipalities distributed across 13 microregions.

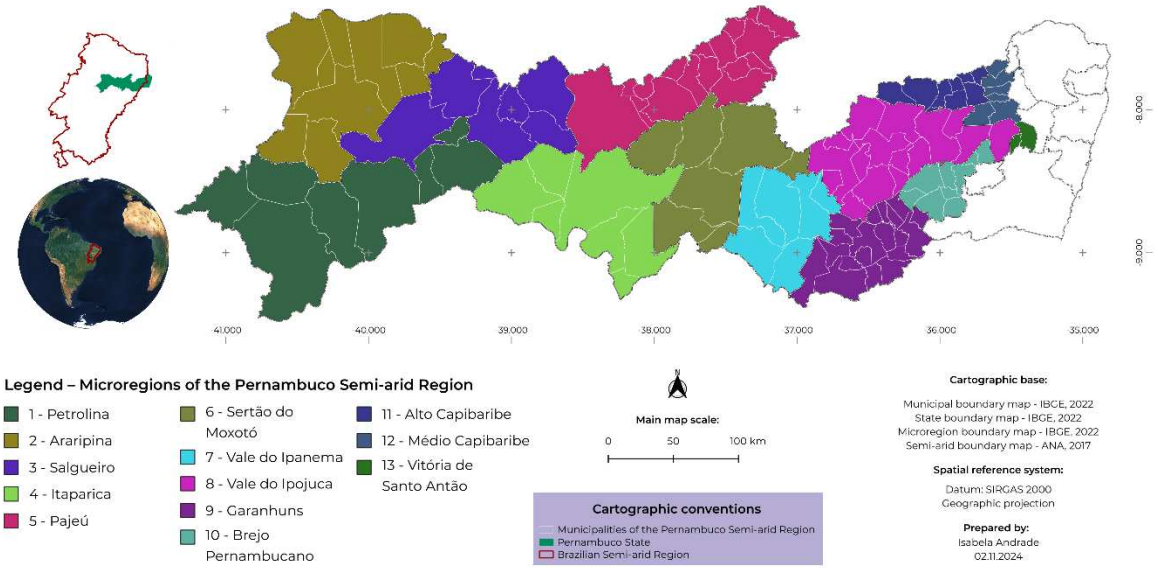


Fig. 1 Geographical location of the study area in the Pernambuco Semiarid region and its division into microregions. The map, prepared by the authors from IBGE (2017) and SUDENE (2017) data,

shows the 13 microregions used in the analyses of thermal extremes. Geographic reference system: SIRGAS 2000

This delimitation is justified by the need to maintain spatial consistency in the analyzed historical series (1994–2023), avoiding discontinuities associated with territorial changes over time. The analyses were conducted at the microregion and municipal scale and Fig. 2 depicts the methodological flowchart.

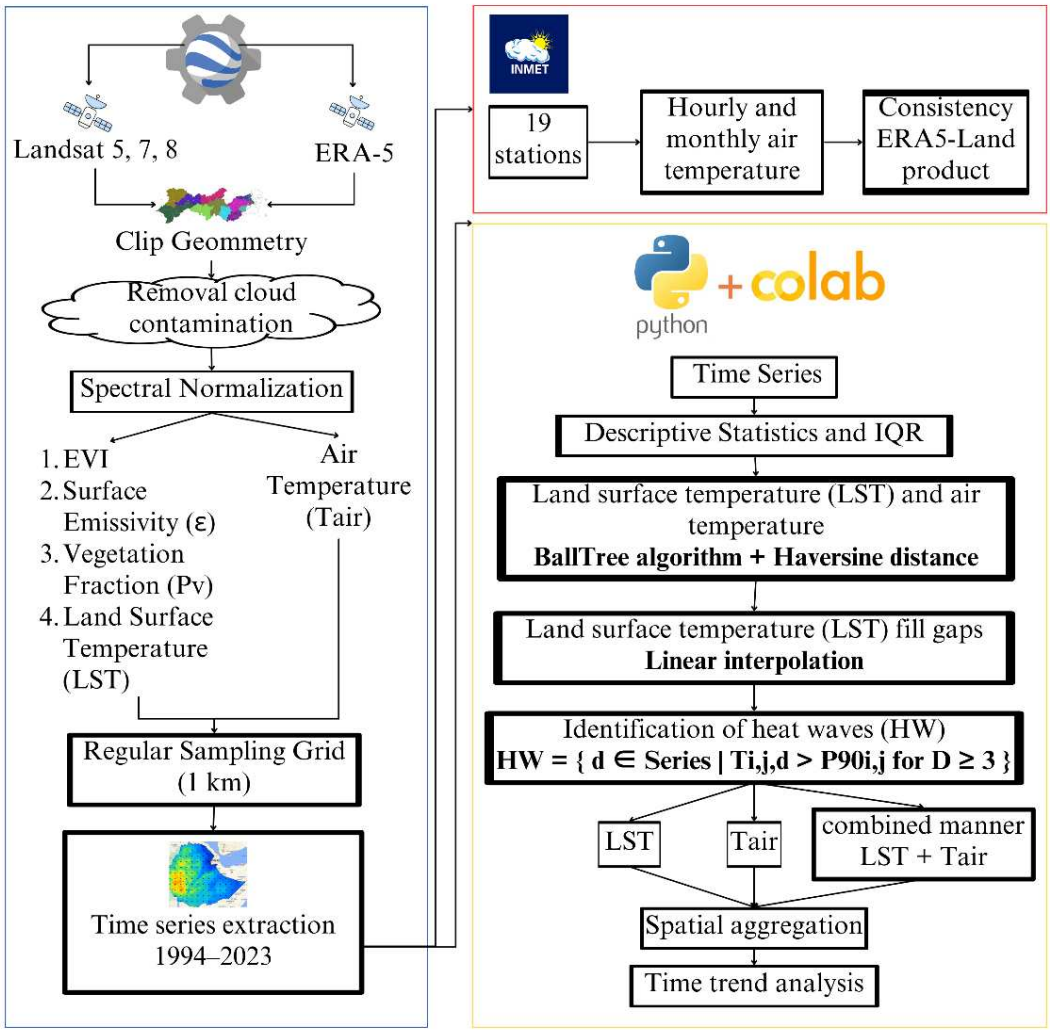


Fig. 2 Schematic diagram of the methodology

2.2 Satellite data and processing in Google Earth Engine

The satellite imagery was processed on the Google Earth Engine (GEE) platform, which enables large-scale geospatial analysis through cloud computing (Gorelick et al. 2017). Images from the Landsat-5 TM (1994–2011), Landsat-8 OLI/TIRS (2013–2023), and Landsat-9 OLI-2/TIRS-2 (2021–2023) sensors were used, all from Collection 2, Tier 1 ('LANDSAT/LT05/C02/T1_TOA','LANDSAT/LC08/C02/T1_TOA',and 'LANDSAT/LC09/C02/T1_TOA') (Ermida et al. 2020; Crawford et al. 2023). The thermal bands (native resolution of 120 m for TM and 100 m for TIRS) are distributed resampled to 30 m, and each satellite has a nominal revisit time of 16 days; an 8-day interval occurs only when Landsat-8 and Landsat-9 operate together (from late 2021 onwards).

Preprocessing included spatial clipping of the study area, removal of cloud-contaminated pixels using the quality assessment band (QA_PIXEL), and spectral standardization across sensors, enabling integration of the time series. From these images, the following variables were derived: the Enhanced Vegetation Index (EVI) (Eq. 1), used to estimate vigor and density of vegetation cover with lower influence of soil and spectral saturation in densely vegetated areas (Liu and Huete 1995); the vegetation fraction (Pv) (Eq. 2), which represents the proportion of vegetation cover present on the surface and supports the biophysical characterization of the terrain; the surface emissivity (ε) (Eq. 3), a key parameter to describe the capacity of the surface to emit thermal radiation and to reduce uncertainties in thermal estimation (Chen et al. 2019); and the Land Surface Temperature (LST) (Eq. 4), used to evaluate the thermal dynamics of the surface and to identify warming patterns associated with heat waves and environmental stress (Kodimalar et al. 2020).

$$EVI = 2.5 \times \frac{NIR - RED}{NIR + 6 \times RED - 7.5 \times BLUE + 1} \quad (1)$$

$$P_v = \left[\frac{EVI - EVI_{min}}{EVI_{max} - EVI_{min}}\right]^2 \quad (2)$$

$$\varepsilon = 0.004 \times P_v + 0.960 \quad (3)$$

$$LST = \frac{BT}{\left[1 + \left(\frac{10.8 \times BT}{14380}\right) \times ln(\varepsilon)\right]} \quad (4)$$

where NIR, RED, and BLUE represent the spectral bands; BT is the brightness temperature; and ε is the surface emissivity.

2.3 Climate data (ERA5) and validation

The air temperature was obtained from the ERA5 atmospheric reanalysis, produced by the European Centre for Medium-Range Weather Forecasts within the Copernicus Climate Change Service (C3S). The data were extracted from the collection available on Google Earth Engine ('ECMWF/ERA5/HOURLY'), transformed to daily averages, and from the Copernicus Climate Data Store (CDS). ERA5 is a fifth-generation climate reanalysis product, developed by integrating meteorological observations from surface stations, radiosondes, satellites, ocean buoys, and aircraft into global numerical atmospheric models. This process combines observational measurements and atmospheric physical modeling, enabling the generation of continuous, spatially consistent time series with reduced observational gaps (Hersbach et al. 2020; Bell et al. 2021).

The variable used was the 2 m air temperature, a parameter widely used to represent near-surface thermal conditions and their impacts on thermal comfort, ecosystems, and extreme events. The ERA5 collection has a spatial resolution of about 31 km and provides hourly and aggregated estimates of air temperature. ERA5 has been widely used in climate studies, environmental

monitoring, and analyses of thermal extremes at regional and global scales (Hersbach et al. 2020; Bell et al. 2021; Xu et al. 2022).

The choice of ERA5 is justified by its high temporal consistency, continuous spatial coverage, and recognized reliability in representing atmospheric variables, particularly in regions with low density of meteorological stations, such as areas of the Brazilian Semiarid region (Araújo et al. 2022). In addition, integrating meteorological observations with numerical modeling improves the robustness of spatio-temporal analysis of thermal variability, enabling identification of the frequency, intensity, and persistence of extreme heat events across the analyzed historical series.

The consistency of these data was assessed by comparing them with observational records from automatic meteorological stations of the National Institute of Meteorology (INMET) in the Pernambuco Semiarid region, using the Pearson correlation coefficient, mean error, root mean square error, and bias, calculated for maximum and minimum temperatures. Hourly and monthly air temperature data from 19 automatic and conventional INMET stations in the semiarid region of Pernambuco were used (Bezerra et al. 2019). For the semiarid region of Pernambuco (≈86,341 km²), for the semiarid region of Pernambuco (≈86,341 km²), Araújo et al. (2022, 2025) validated ERA5-Land against only eight automatic INMET stations. This highlights the low density of meteorological stations in the region, which, compared with studies in other regions of Brazil and Europe, reinforces the need to complement point observations with reanalysis products in regional climate studies (Araújo et al. 2022).

2.4 Data organization and processing

Before variable extraction, a regular sampling grid with 1 km spatial resolution was established across the entire study area, enabling standardized analysis units and consistent

integration across datasets. For each grid cell, spectral and thermal variables derived from Landsat images were extracted, along with ERA5 air temperature data, ensuring spatial correspondence between the sources.

The data extracted from Google Earth Engine (GEE) were processed in a Python environment (Google Colab), in line with workflows that integrate GEE with interactive notebooks (Tamiminia et al. 2020; Wu 2020). Initially, the series were organized into a structured database with standardized variables, dates, and spatial identifiers. Subsequently, the data were stored in the Apache Parquet columnar format to reduce I/O (input/output) costs and optimize computational performance for analytical operations on large data volumes (Zeng et al. 2023).

Descriptive statistics (mean, median, minimum and maximum values, and standard deviation) were calculated as a preliminary step of quality control and exploration of the series, following well-established practices in the quality assurance and quality control (QA/QC) of meteorological data. The detection of extreme values was performed using the interquartile range (IQR) method, a non-parametric approach widely employed in environmental data quality control due to its robustness to asymmetric distributions and long tails. The exclusion of outliers was applied judiciously, restricted to values associated with land use and land cover classes not representative of the analysis (for example, water bodies and urban areas) or to thermally implausible values for the study region, in agreement with studies that use the IQR to remove statistical anomalies reflecting measurement errors or atypical site conditions, while preserving physically plausible extreme events (Faybishenko et al. 2021).

2.5 Data integration and temporal reconstruction of LST

The integration between land surface temperature (LST) and air temperature was performed by spatial pairing using the nearest neighbor method, applying the BallTree algorithm

with the Haversine distance (Dumitrescu et al. 2020). Owing to the temporal irregularity of the Landsat imagery, a pixel-wise linear temporal interpolation was applied to fill gaps of up to 32 days, conditional on the existence of adjacent observations (Liu et al. 2020; Mo et al. 2021). The accuracy of the reconstruction was assessed by cross-validation, using mean absolute error (MAE), root mean square error (RMSE), and bias (Shiff et al. 2021), in addition to the estimation of 95% confidence intervals for the analysis of uncertainty.

2.6 Identification of heat waves

The identification of heat waves was performed for each pixel of the time series, using relative thresholds based on the 90th percentile (P90) of the local climatology (Perkins and Alexander 2013). An event was defined as a period of at least three consecutive days in which the temperature exceeded this threshold (Eq. 5).

$$HW = \left\{ d \in Series \mid T_{i,j,d} > P90_{i,j} \; for \; D \geq 3 \right\} \quad (5)$$

Detection was applied separately to the land surface temperature (LST) and air temperature (Tair) series, as well as in a combined manner, considering only simultaneous events. The events were characterized in terms of frequency, duration, and magnitude, the latter defined as the sum of the thermal anomalies relative to the threshold (Hu et al. 2023).

2.7 Trend analysis and spatial aggregation

The temporal trends in heat waves were assessed from annual series derived from pixel-wise event detection. Initially, for each pixel of the sampling grid, the annual frequency of heat wave occurrence was calculated. Subsequently, to reduce the influence of local thermal noise and ensure the spatial representativeness of the events, a spatial aggregation criterion was applied, selecting only contiguous clusters with a minimum area of 1 km as valid events.

This procedure allowed isolated occurrences associated with specific targets of high thermal response, such as rocky outcrops, artificial surfaces, or anomalous pixels, to be filtered out, ensuring that the identified events represented consistent spatial patterns of extreme heat. From these clusters, annual series of frequency, duration, and magnitude of heat waves were generated and used in the subsequent analyses.

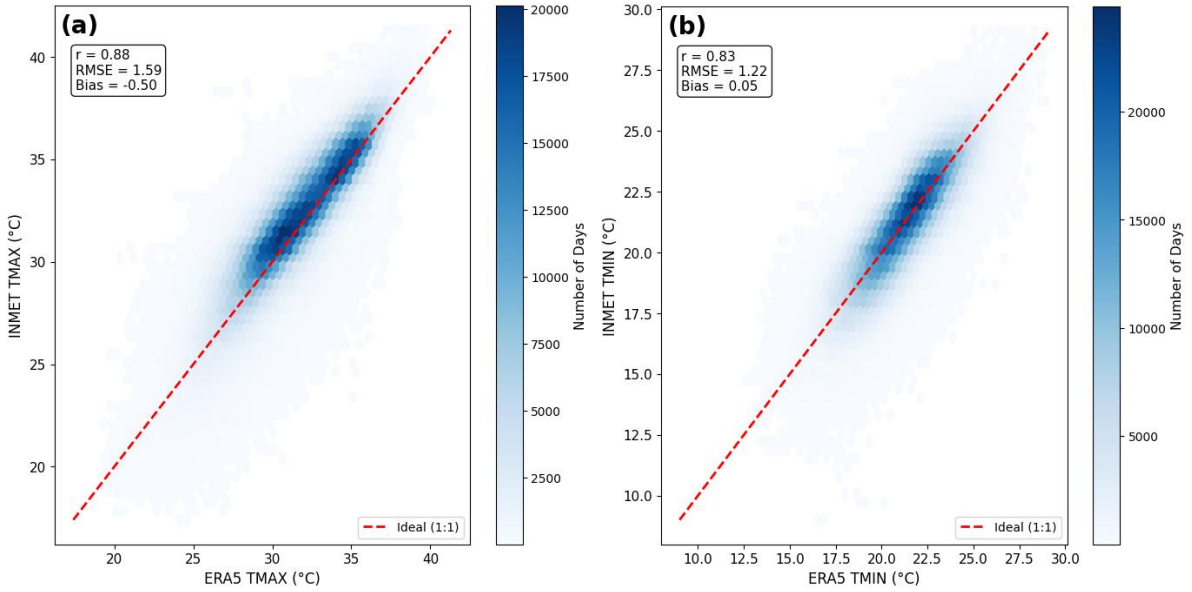
The temporal trends of these metrics were evaluated using the non-parametric Mann–Kendall test, adopting a significance level of 5% ($\alpha = 0.05$), while the magnitude of the trends was estimated using Sen's method (Perkins-Kirkpatrick and Lewis 2020; Chang et al. 2021). The analyses were performed separately for the series derived from land surface temperature (LST) and air temperature (Tair), allowing the investigation of possible differences associated with soil-atmosphere coupling (Karinou et al. 2025).

3 Results and discussion

The results are presented in sequence, from data reliability to long-term spatio-temporal patterns of heat waves in the Pernambuco Semiarid region.

3.1 Performance of ERA5 air temperature

The validation of the maximum and minimum air temperatures from ERA5 was carried out by comparing the reanalysis data with INMET observations in 11 municipalities of the Pernambuco Semiarid region (Fig. 3). The results show high consistency between the reanalysis product and the in situ observations, indicating that ERA5 adequately represents the regional thermal conditions.



237

238 **Fig. 3** Cross-validation of daily ERA5 air temperature against INMET station observations: (a)
239 maximum temperature and (b) minimum temperature. The red dashed line is the 1:1 line; colors
240 indicate the density of occurrences (days), from light blue (low frequency) to dark blue (high
241 frequency). r, Pearson correlation coefficient; RMSE, root mean square error

242 For maximum air temperature (Fig. 3a), a strong linear correlation (r = 0.88) and a root
243 mean square error (RMSE) of 1.59 °C were observed, indicating good performance of the
244 reanalysis product in representing daily in situ temperature measurements. These values lie within
245 the reliability range reported for Northeastern Brazil. Araújo et al. (2025), when validating ERA5-
246 Land data in Pernambuco, also reported high coefficients of determination (often greater than 0.90)
247 and RMSE values ranging from 0.40 °C to 1.98 °C, reinforcing the product's capacity to reproduce
248 regional thermal variability adequately.

249 Despite the overall good performance, a systematic negative bias of −0.50 °C was
250 identified in the maximum temperatures (Fig. 3a), indicating a slight underestimation of heat peaks
251 by ERA5. This behavior is consistent with patterns already documented in different regions of the
252 world, including Europe, China, Portugal, and southern Africa (Velikou et al. 2022; Xu et al. 2022;

Almeida and Coelho 2023; Roffe and van der Walt 2023). Such underestimation is widely attributed to the spatial smoothing inherent to reanalyses, in which each pixel represents an average over areas of tens of kilometers, reducing the representation of point extremes.

In the context of the Semiarid region, Silva et al. (2025) emphasize that this smoothing arises from the difference between the spatial scale of the model and the microclimatic variability observed at the surface, often intensified by exposed soil, heterogeneity of the vegetation cover, and urbanization. Thus, while meteorological stations capture extreme local conditions, ERA5 represents average regional conditions, which explains the attenuation of the maximum values.

For minimum air temperature (Fig. 3b), ERA5 also performed well, with $r = 0.83$ and RMSE of 1.22 °C, indicating that ERA5 reproduces the day-to-day variability of nighttime minima reasonably well. This result reinforces the suitability of the product for regional climatological studies, especially in areas with low observational density. Araújo et al. (2022) also reported good performance of the thermal variables in the state of Pernambuco, with high coefficients of determination and moderate errors, indicating the reliability of the reanalysis for studies of climatic variability in the Semiarid region.

3.2 Surface and air temperature dynamics

The LST mean in the microregions of the Pernambuco Semiarid region (Table 1) ranged from 26.58 °C (Vitória de Santo Antão) to 29.34 °C (Vale do Ipanema), indicating a regional pattern of elevated, relatively homogeneous temperatures, but with pronounced thermal extremes. This behavior is consistent with that observed in areas of the Caatinga biome, where the combination of low vegetation cover and predominance of exposed soil favors the accumulation of energy at the surface. Jardim et al. (2022) emphasize that such conditions may lead to markedly

elevated surface temperatures during severe drought events, reflecting the high thermal sensitivity of this environment to variations in soil moisture and land cover.

The extreme values reinforce this pattern, with records exceeding 47 °C in all microregions of the Sertão, reaching 48.00 °C in Araripina and Salgueiro (Table 1). These results show the capacity of the surface-soil system of the Semiarid region to reach critical warming levels under conditions of high solar radiation and low water availability.

The wide temperature range and the relatively high standard deviations of LST (~4.8 °C to 6.1 °C) indicate strong spatio-temporal variability associated with the low thermal inertia of dry soil. On surfaces with little moisture and vegetation, radiative energy is predominantly converted into sensible heat, while latent heat flux is reduced, favoring rapid daytime warming and pronounced nighttime cooling (Yu et al. 2021).

Table 1 Descriptive statistics of Land Surface Temperature (LST) data by microregion of the Pernambuco Semiarid region (1994–2023)

Microregion	Mean (°C)	Median (°C)	Minimum (°C)	Maximum (°C)	Std. Deviation (°C)
Alto Capibaribe	28.22	27.93	8.01	47.95	5.58
Araripina	29.07	29.06	8.00	48.00	5.87
Brejo Pernambucano	27.68	27.22	8.03	47.96	5.48
Garanhuns	28.52	28.30	8.02	47.98	5.90
Itaparica	29.24	29.23	8.00	47.99	5.98
Médio Capibaribe	27.27	26.66	8.01	47.64	5.15
Pajeú	29.09	29.19	8.00	47.98	6.02
Petrolina	29.07	29.12	8.00	47.99	5.56
Salgueiro	29.26	29.23	8.00	48.00	5.89
Sertão do Moxotó	29.27	29.23	8.00	47.99	6.07
Vale do Ipanema	29.34	29.22	8.00	47.99	6.11
Vale do Ipojuca	28.23	27.95	8.01	47.96	5.71
Vitória de Santo Antão	26.58	25.92	8.01	47.63	4.80

Note: The statistics were calculated from a historical series of Landsat satellite imagery, which reflects land surface temperature (LST). "Minimum" and "Maximum" indicate the absolute extremes found in the microregion. "Std. Deviation" indicates the variability of the data relative to the mean.

The LST extremes reported here should be interpreted in light of potential uncertainties associated with the retrieval and processing procedures, including emissivity estimation, atmospheric effects, and the integration of different Landsat sensors. Although these factors may influence temperature estimates, they do not, by themselves, establish fixed lower or upper temperature limits. The clustering of minimum and maximum values near 8 and 48 °C,

297 respectively, therefore warrants verification of the quality-control criteria and any range-based
298 filtering applied during processing. Until their influence is quantified, these values should be
299 regarded as the extremes of the processed dataset rather than physical temperature limits of the
300 study region. Any implications for percentile-based thresholds and heat-wave metrics also require
301 sensitivity analysis.

302 In contrast, air temperature (Table 2) showed a more homogeneous and damped behavior.
303 The means ranged from 28.10 °C to 32.03 °C, while the standard deviations (~2.3 °C to 3.2 °C)
304 were approximately half of those observed for LST. The maximum air temperatures (~40 °C) were
305 also markedly lower than the surface maxima (~48 °C), indicating thermal decoupling between
306 the surface and the near-surface atmosphere.

Table 2 Descriptive statistics of Air Temperature (Tair) data by microregion of the Pernambuco Semiarid region (1994–2023)

Microregion	Mean (°C)	Median (°C)	Minimum (°C)	Maximum (°C)	Std. Deviation (°C)
Alto Capibaribe	29.77	29.97	20.37	37.12	2.48
Araripina	31.27	31.21	20.02	39.67	2.79
Brejo Pernambucano	28.07	28.20	19.43	35.83	2.58
Garanhuns	28.82	28.84	18.75	39.05	3.19
Itaparica	32.00	32.11	20.66	40.08	2.99
Médio Capibaribe	28.91	29.02	20.51	36.24	2.39
Pajeú	31.80	31.94	19.72	39.91	2.90
Petrolina	32.03	32.02	21.34	40.11	2.65
Salgueiro	31.77	31.74	20.09	39.91	2.88
Sertão do Moxotó	31.48	31.67	19.32	40.08	3.12
Vale do Ipanema	30.63	30.88	18.75	39.36	3.20
Vale do Ipojuca	29.07	29.22	18.75	37.77	2.77
Vitória de Santo Antão	28.10	28.18	20.51	35.12	2.28

Note: The values refer to the 2 m air temperature (°C), obtained from the ERA5 climate reanalysis. The mean represents the climatology of the period (1994–2023), while the maximum and minimum values correspond to the daily extremes identified by the model within each microregion. "Std. Deviation" indicates the variability of the data relative to the mean.

This magnitude difference (~8 °C between the surface and air extremes) is consistent with classical thermal decoupling processes under conditions of atmospheric stability. Previous work also suggests that, in semiarid regions, LST tends to exhibit greater temporal variability and a

316 larger thermal amplitude compared to air temperature, due to the lower thermal damping of the
317 surface (Bindajam et al. 2020).

318 In addition to the physical processes, part of this difference in variability is associated with
319 the distinct spatial scales of the products used. The Landsat-derived LST (30 m) captures local
320 heterogeneities such as mosaics of vegetation, exposed soil, and anthropogenic uses, amplifying
321 the observed spatial variability. The air temperature from the ERA5 reanalysis (~31 km), in turn,
322 represents regional-scale spatial averages, smoothing local gradients and reducing apparent
323 variability (Hersbach et al. 2020; Zhang et al. 2024). The greater variability of LST results from
324 both its higher physical sensitivity to local conditions and the higher spatial resolution of optical
325 remote sensing, compared with the spatially integrated character of atmospheric reanalysis data.

326 **3.3 LST reconstruction**

327 The reconstruction of the LST time series by linear interpolation showed a satisfactory
328 overall performance in filling gaps in the Pernambuco Semiarid region, presenting a mean bias
329 close to zero (0.04 °C). This result indicates no systematic bias in the mean, although a near-zero
330 mean bias does not establish the accuracy of the reconstructed extremes (Table 3).

331 Despite satisfactory aggregate performance, the validation metrics (Table 3) reveal strong
332 spatial heterogeneity in reconstruction quality, indicating that uncertainty is controlled by local
333 surface and atmospheric conditions. The performance ranged from high reliability in Vale do
334 Ipojuca (RMSE ~ 2.66 °C; r = 0.92) to low reliability in Sertão do Moxotó (RMSE ~ 6.19 °C; r =
335 0.55), showing that performance is not spatially uniform.

Table 3 Statistical performance metrics of the validation of the Land Surface Temperature (LST) data by microregion of the Pernambuco Semiarid region

Microregion	Samples	MAE (°C)	RMSE (°C)	r (Pearson)	Bias (°C)	Std. Deviation (°C)	Uncert. 95% (±°C)
Alto Capibaribe	26,991	1.45	4.14	0.74	0.13	4.13	8.11
Araripina	43,320	1.84	3.50	0.81	0.03	3.45	6.85
Brejo Pernambucano	18,034	1.65	3.23	0.85	−0.02	3.23	6.33
Garanhuns	26,714	3.36	5.86	0.65	0.06	5.86	11.48
Itaparica	52,042	3.12	4.71	0.66	−0.02	4.71	9.23
Médio Capibaribe	10,473	3.01	4.04	0.67	−0.02	4.04	7.92
Pajeú	77,758	2.21	4.84	0.73	−0.00	4.84	9.48
Petrolina	22,709	3.23	4.36	0.62	−0.12	4.36	8.55
Salgueiro	32,699	2.40	3.81	0.80	−0.08	3.81	7.47
Sertão do Moxotó	46,609	3.55	6.19	0.55	−0.04	6.19	12.14
Vale do Ipanema	31,491	2.32	4.28	0.78	−0.04	4.28	8.38
Vale do Ipojuca	28,357	0.87	2.66	0.92	−0.06	2.65	5.20
Vitória de Santo Antão	16,002	1.65	2.97	0.81	0.09	2.97	5.82
GLOBAL	—	2.36	4.20	0.74	0.04	4.40	8.60

Note: MAE — Mean Absolute Error; RMSE — Root Mean Square Error; r — Pearson Correlation Coefficient. The "95% Uncertainty" column represents the confidence interval of the estimates.

In the microregions of physiographic transition, such as Vale do Ipojuca and Vitória de Santo Antão, the high correlation between the reconstructed series and the reference data ($r > 0.80$) suggests greater thermal stability and better representativeness of the linear interpolation in environments with lower extreme variability. This behavior is consistent with evaluations of

reanalysis products in regions of low observational density, in which seasonal thermal patterns are well captured. However, biases in extreme magnitude persist (Roffe and van der Walt 2023).

In contrast, in the Sertão do Moxotó and Pajeú, regions with the largest water deficits in the state, the errors and standard deviations were high (RMSE of 6.19 °C and 4.84 °C, respectively), reflecting the high surface thermal instability associated with the predominance of exposed soil. In these environments, the low thermal inertia causes the surface to respond rapidly to incident radiation, resulting in strong daily variability and reducing the capacity of interpolative methods to capture abrupt extremes. This behavior is typical of semiarid environments with reduced vegetation cover, where the energy balance is dominated by sensible heat flux at the expense of latent heat, intensifying the surface thermal amplitude (Martins et al. 2025).

The analysis of the residuals indicates the presence of two distinct systematic patterns among the microregions. In Petrolina (−0.12 °C) and Salgueiro (−0.08 °C), a slight underestimation of the thermal peaks is observed, associated with the typical behavior of linear interpolation methods, which tend to smooth extremes by imposing temporal continuity and reducing high-frequency variability (Wu et al. 2019). This effect dampens acute surface warming events.

On the other hand, in Alto Capibaribe (+0.13 °C), the positive bias may be related to the so-called *clear-sky bias*, in which LST estimates based on thermal sensors are influenced by a higher frequency of observations under clear-sky conditions, leading to a relative overestimation of the mean temperature when cooling events associated with cloudiness are not fully sampled. Likewise, the presence of clouds, which reduces the availability of valid observations, increases reliance on interpolation and amplifies uncertainties in the representation of thermal extremes (Holmes et al. 2016).

Although the reconstruction showed a near-zero mean bias, this does not establish the reliability of individual temperature extremes or threshold-based event detection. The reported reconstruction errors warrant particular caution when interpreting low-intensity LST events. Consequently, the frequency, duration, and intensity of events derived from the interpolated series should be regarded as provisional pending event-focused validation and sensitivity analyses addressing gap length and reconstruction uncertainty.

3.4 Detection and temporal evolution of heat waves

The analysis of the annual frequency of heat waves in the Pernambuco Semiarid region (1994–2023) shows strong interannual variability and different behavior at the surface and in the atmosphere. The comparison between the absolute pixel count (Fig. 4a) and the identification of spatially aggregated regional systems (Fig. 4b) indicates that the phenomenon is not restricted to point anomalies, but is organized as spatially coherent events at the regional scale.

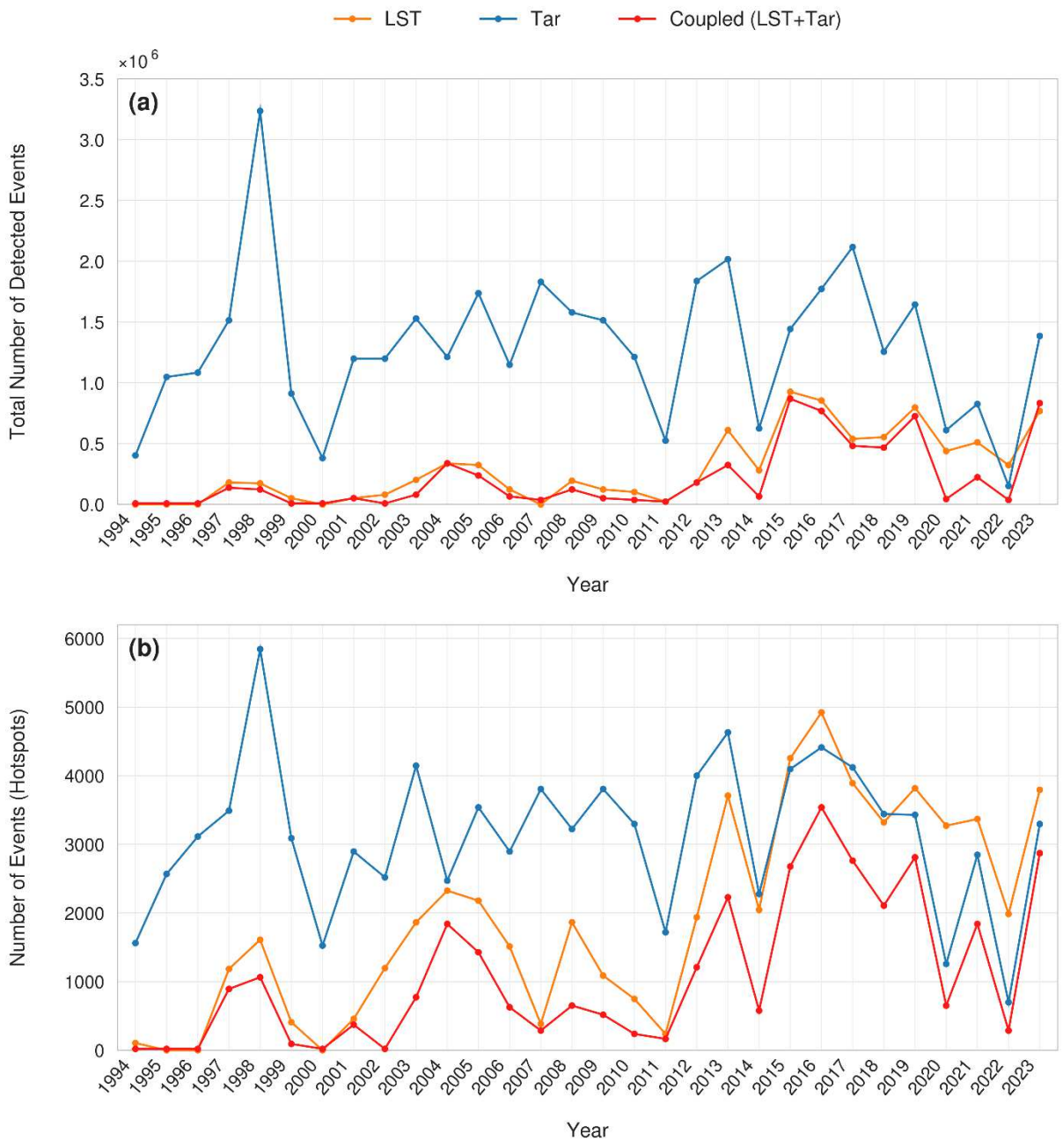


Fig. 4 Temporal evolution of the annual frequency of heat waves in the Pernambuco Semiarid region (1994–2023): (a) absolute pixel count; (b) clusters with a minimum area greater than 1 ha. Tair (air) values are derived from the ERA5 reanalysis and LST values from the Landsat time series. In (a), the scale in 10^6 reflects the total number of pixels classified as heat wave in each

year; in (b), the count refers to clusters of neighboring pixels, filtered to retain only events larger than 1 ha in order to remove small-scale thermal noise.

Extreme atmospheric events (Tair) show a strong association with large-scale warm phases, particularly during El Niño episodes. In 1998, associated with a strong El Niño event, the historical peak of atmospheric systems is observed (approximately 5,900 regional events), highlighting the sensitivity of the atmosphere to large-scale climate forcings. During this period, the surface response (LST) showed a lower relative intensity, suggesting thermal decoupling between the soil and the atmosphere.

This pattern is consistent with evidence of greater structural integrity of the vegetation cover in the late 1990s, when vegetation still played a relevant role in modulating the surface energy balance. Biomass and soil moisture increase latent heat flux and reduce extreme surface warming, acting as a thermal-damping mechanism.

The temporal evolution from 2001 to 2007 revealed distinct behavior between the variables: the air temperature shows greater interannual variability, while the LST responds more slowly and persistently. This pattern is consistent with the presence of soil thermal inertia and the hydrothermal memory of the surface, already described in classical studies of soil-atmosphere interaction (Seneviratne et al. 2010). This temporal decoupling indicates that the land surface acts as a slow-response thermal reservoir, modulating the persistence of heat states even after the passage of short-duration atmospheric forcings.

From approximately 2013 onwards, however, a structural change in the regional thermal system is observed, characterized by convergence between the Tair and LST series and by the simultaneous increase in the frequency of extreme events in both variables. This behavior is consistent with the intensification of the prolonged drought in the Northeast between 2012 and

2017, widely documented as one of the most severe hydrometeorological events of the century (CEMADEN 2018).

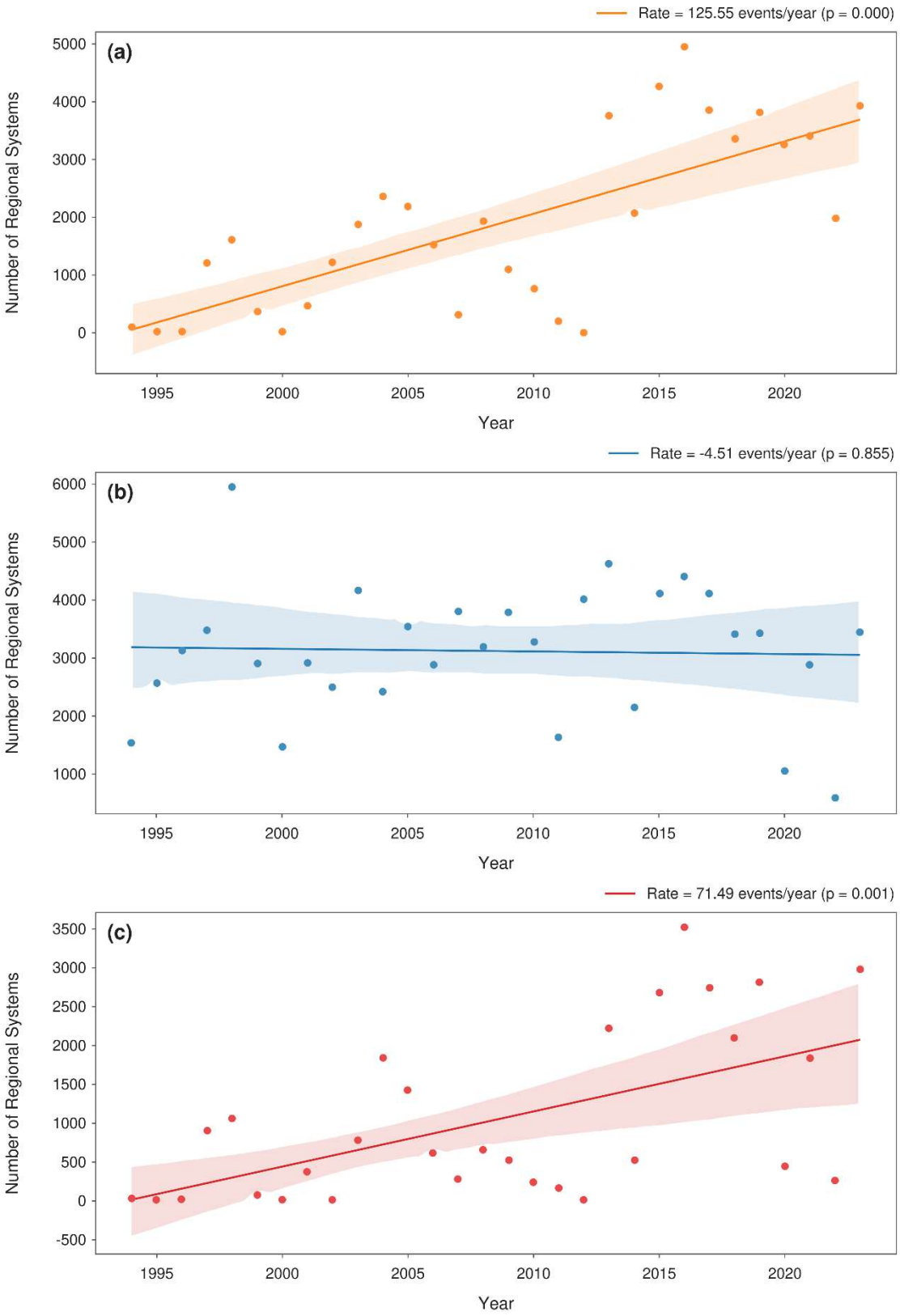
During this period, the surface began to show greater persistence of elevated thermal states, indicating a reduction in the biophysical regulation capacity of the soil-vegetation system. The relative increase in the frequency of LST events compared to Tair between 2015 and 2019 suggests that the surface began to play an active role in maintaining regional thermal stress, rather than acting solely as a passive response to the atmosphere.

The recent inversion between LST and Tair (2015–2019), characterized by the predominance of surface events, indicates the strengthening of soil-atmosphere feedback mechanisms. In this process, surface warming intensifies the warming of the atmospheric boundary layer and vice versa, a mechanism that has been associated with the amplification of heat waves in semiarid and dry systems (Miralles et al. 2014). In this interpretation, the surface would contribute to maintaining and amplifying extreme events rather than only responding to them; this feedback was not quantified here.

The absence of LST events in 2012 does not reflect a physical absence of warming, but rather an instrumental gap associated with the transition between Landsat-5 and Landsat-8 missions. Landsat-5 TM stopped acquiring images in November 2011, and Landsat-7 ETM+ has operated with its Scan Line Corrector off (SLC-off) since 2003, which compromises the continuity of spatial coverage (Wulder et al. 2011; Wijedasa et al. 2012). The launch of Landsat-8 in 2013, carrying the Thermal Infrared Sensor (TIRS) with two thermal bands, restored the thermal record, and the addition of Landsat-9 data from 2022 (USGS 2022) halved the revisit interval to 8 days. Consequently, the higher frequency of recorded LST events in the post-2013 period may partially reflect improved detectability, rather than an abrupt physical intensification of surface warming.

3.5 Long-term trends in heat wave frequency

The comparative analysis of the linear regression lines for the three event categories (Fig. 5) shows a clear contrast in the Pernambuco Semiarid region: atmospheric heat waves vary from year to year without a trend, whereas surface heat waves increase.


Rate = 125.55 events/year (p = 0.000)
(a)
Number of Regional Systems
5000
4000
3000
2000
1000
0
1995
2000
2005
2010
2015
2020
Year
Rate = -4.51 events/year (p = 0.855)
(b)
Number of Regional Systems
6000
5000
4000
3000
2000
1000
1995
2000
2005
2010
2015
2020
Year
Rate = 71.49 events/year (p = 0.001)
(c)
Number of Regional Systems
3500
3000
2500
2000
1500
1000
500
0
-500
1995
2000
2005
2010
2015
2020
Year

435

Fig. 5 Long-term trends of heat waves in the Pernambuco Semiarid region (1994–2023): (a) surface heat waves (LST); (b) atmospheric heat waves (Tair); (c) coupled heat wave events (LST + Tair)

The time series of purely atmospheric heat waves (Fig. 5b) does not show a statistically significant trend over the 30 analyzed years (p-value = 0.855). The rate of change of −4.51 events/year suggests that air temperature extremes in the region continue to operate under a regime of cyclical climatic fluctuations, strongly influenced by modes of natural variability such as ENSO (El Niño–Southern Oscillation), without a systematic increase in frequency.

In contrast, surface heat waves (Fig. 5a) showed a significant increase (p-value < 0.001), with a trend of more than 100 events per year across the Pernambuco Semiarid region. This increment refers to the total number of events identified in the study area, considering the set of analyzed pixels, and indicates the spatio-temporal intensification of extreme heat conditions in the region. This pattern is consistent with changes in the surface energy balance associated with reduced vegetation cover and increased sensible heat flux, which were not measured here. In the Petrolina region, this temperature pattern can be explained by the large extent of exposed soil, degraded pasture, and agricultural areas, which exhibit substantially higher LST values (Jardim et al. 2022).

The replacement of native vegetation by non-evaporative land uses increases the sensible heat flux and raises LST to approximately 48–52 °C during dry years. Duveiller et al. (2018) quantified globally that vegetation transitions, particularly deforestation and conversion to agriculture in tropical dry regions, lead to an average increase in LST due to reduced transpiration and increased sensible heat flux, even when surface reflectance increases. The scenario in which surface and air extremes coincide (Fig. 5c) also showed a significant upward trend (p-value =

0.001), with an increase of more than 70 events per year across the Pernambuco Semiarid region. The increase in coupled events may indicate shorter periods of thermal relief for the vegetation; the proposed feedback from heated soil to the atmospheric boundary layer was not tested in this study.

3.6 Long-term trends in heat wave metrics

The application of the Mann–Kendall test revealed a consistent divergence in the trends of heat waves between air and surface temperatures (Tables 4–7). While atmospheric events did not show a statistically significant trend over the analyzed period (p-value > 0.05), behaving as interannual fluctuations, surface heat waves exhibited a robust and significant increase, especially in frequency and duration (p-value < 0.01) (Table 4).

Table 4 Temporal trend analysis (1994–2023) of surface, atmospheric, and coupled heat wave metrics in the Pernambuco Semiarid region

Event	Metric	Trend (annual)	p-value
Heat Waves — Surface	Frequency	102.28	<0.01**
	Duration	0.27	<0.01**
	Magnitude	0.32	0.63 ns
Heat Waves — Atmosphere	Frequency	−13.34	0.82 ns
	Duration	0.01	0.69 ns
	Magnitude	0.01	0.66 ns
Coupled Events	Frequency	74.76	<0.01**
	Duration	0.07	0.05*
	Magnitude	0.42	0.08 ns

Note: The Trend column indicates the mean rate of increase or decrease of the metric per year. The p-value evaluates the statistical significance of the trend. (*) indicate a significant trend at

the 95% confidence level; (**) indicate a significant trend at the 99% confidence level; and (ns) indicates non-significant.

The spatial analysis reinforces the idea that this trend is not uniform across the Pernambuco Semiarid region. In the case of atmospheric events, an unstable behavior is observed, with predominantly non-significant or negative trends across several microregions (Table 5). In areas such as Garanhuns, Pajeú, and Sertão do Moxotó, the frequency of atmospheric heat waves shows significant reductions ($p \leq 0.02$), indicating the strong influence of interannual climate variability.

Table 5 Spatial trends of frequency, duration, and magnitude of atmospheric (Tair) heat waves by microregion (1994–2023)

Microregion	Frequency (Events/year)	p (Freq)	Duration (Days/year)	p (Dur)	Magnitude (Load/year)	p (Mag)
Alto Capibaribe	20.83	0.45	0.01	0.07	0.01	0.10 (ns)
Araripina	41.08	0.00	0.00	0.85	0.02	0.01
Brejo Pernambucano	26.51	0.34	0.02	0.01	0.02	0.04
Garanhuns	−46.51	0.01	0.03	0.00	0.03	0.00
Itaparica	−29.04	0.06	−0.01	0.27	0.00	0.72 (ns)
Médio Capibaribe	28.05	0.38	−0.01	0.58	0.00	0.97 (ns)
Pajeú	−38.72	0.02	−0.01	0.33	0.00	0.99 (ns)
Petrolina	12.13	0.34	0.01	0.11	0.02	0.08 (ns)
Salgueiro	12.51	0.30	0.00	0.59	0.01	0.21 (ns)
Sertão do Moxotó	−51.23	0.00	0.01	0.26	0.01	0.27 (ns)
Vale do Ipanema	−69.92	0.00	0.02	0.00	0.02	0.04
Vale do Ipojuca	−10.34	0.51	0.03	0.00	0.03	0.00
Vitória de Santo Antão	42.25	0.29	0.01	0.37	0.02	0.45 (ns)

Note: The values represent the slope of the regression line. (ns) indicates a statistically non-significant trend (p-value > 0.05).

In contrast, surface heat waves show consistent growth across all microregions (Table 6). The frequency and duration of events increased significantly (p-value ≤ 0.01) throughout the study area, with increases of more than 100 events per year in regions such as Pajeú, Petrolina, Salgueiro, and Itaparica. This pattern indicates a generalized intensification of surface warming, regardless of air temperature behavior.

Table 6 Spatial trends of frequency, duration, and magnitude of surface (LST) heat waves by microregion (1994–2023)

Microregion	Frequency (Events/year)	p (Freq)	Duration (Days/year)	p (Dur)	Magnitude (Load/year)	p (Mag)
Alto Capibaribe	89.63	0.00	0.27	0.00	0.06	0.87 (ns)
Araripina	106.00	0.00	0.31	0.00	0.77	0.00
Brejo Pernambucano	71.69	0.00	0.19	0.00	0.05	0.89 (ns)
Garanhuns	90.89	0.00	0.19	0.00	−0.13	0.59 (ns)
Itaparica	109.44	0.00	0.27	0.00	0.49	0.02
Médio Capibaribe	52.62	0.00	0.26	0.00	0.80	0.00
Pajeú	105.93	0.00	0.26	0.00	0.04	0.88 (ns)
Petrolina	115.52	0.00	0.32	0.00	0.83	0.00
Salgueiro	106.03	0.00	0.30	0.00	0.71	0.00
Sertão do Moxotó	111.15	0.00	0.27	0.00	0.12	0.59 (ns)
Vale do Ipanema	105.03	0.00	0.27	0.00	0.03	0.89 (ns)
Vale do Ipojuca	93.75	0.00	0.20	0.00	−0.15	0.46 (ns)
Vitória de Santo Antão	36.78	0.00	0.21	0.01	0.60	0.13 (ns)

Note: The values represent the slope of the regression line. (ns) indicates a statistically non-significant trend (p-value > 0.05).

Coupled events show an intermediate but more critical pattern (Table 7). The highest growth rates in frequency are concentrated in the Sertão, particularly in the microregions of Pajeú, Salgueiro, and Itaparica, which exhibit increases of more than 100 events per year. In these areas, previously sporadic events have become recurrent, indicating a structural change in the thermal regime.

Table 7 Spatial trends of frequency, duration, and magnitude of coupled heat wave events (LST + Tair) by microregion (1994–2023)

Microregion	Frequency (Events/year)	p (Freq)	Duration (Days/year)	p (Dur)	Magnitude (Load/year)	p (Mag)
Alto Capibaribe	54.12	0.00	0.10	0.00	0.56	0.00
Araripina	100.06	0.00	0.07	0.00	0.42	0.00
Brejo Pernambucano	43.72	0.00	0.08	0.02	0.70	0.00
Garanhuns	47.41	0.00	0.13	0.00	0.69	0.00
Itaparica	103.49	0.00	0.07	0.00	0.57	0.00
Médio Capibaribe	30.15	0.00	0.02	0.30 (ns)	0.25	0.18 (ns)
Pajeú	107.43	0.00	0.08	0.00	0.60	0.00
Petrolina	96.79	0.00	0.08	0.00	0.41	0.00
Salgueiro	102.72	0.00	0.08	0.00	0.52	0.00
Sertão do Moxotó	96.90	0.00	0.08	0.00	0.61	0.00
Vale do Ipanema	73.44	0.00	0.13	0.00	0.60	0.00
Vale do Ipojuca	56.49	0.00	0.10	0.00	0.62	0.00
Vitória de Santo Antão	25.53	0.00	0.00	0.97 (ns)	0.10	0.79 (ns)

Note: The values represent the slope of the regression line. (ns) indicates a statistically non-significant trend (p-value > 0.05).

By contrast, the analysis of the magnitude of coupled events reveals a shift of risk toward transition areas and higher altitudes, such as Brejo Pernambucano and Garanhuns, where the highest rates of thermal intensification are observed (Table 7). This pattern suggests that although the Sertão has the highest frequency of events, regions of the Agreste are experiencing a relative increase in the severity of extreme events.

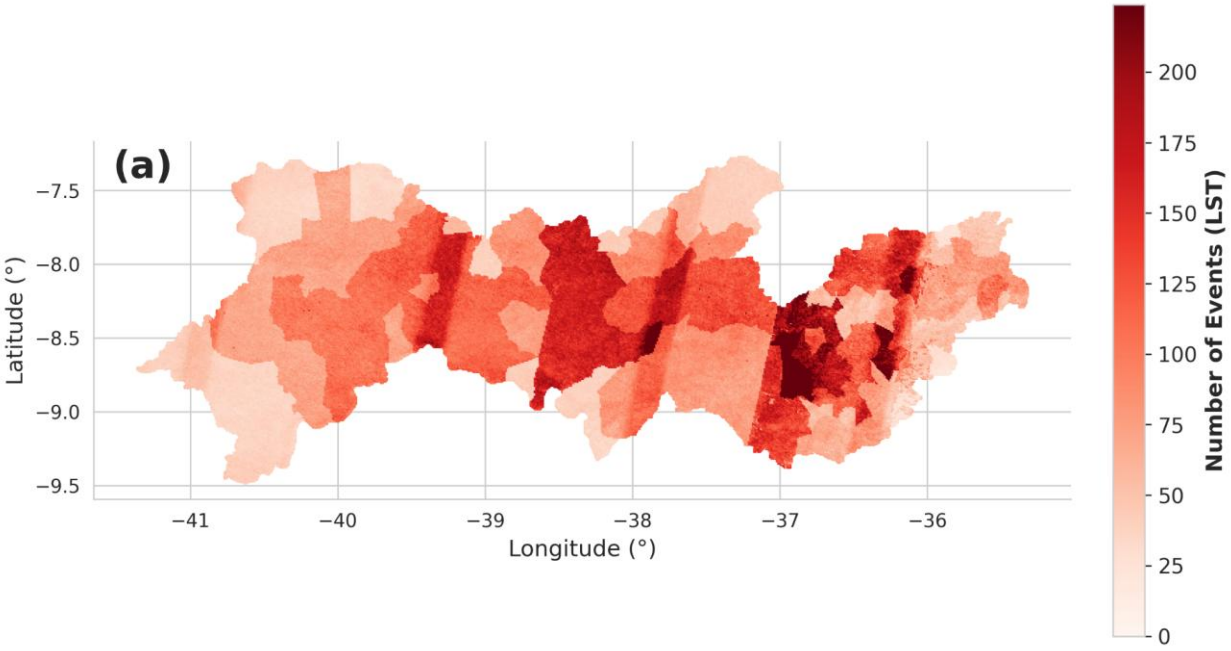
This behavior becomes particularly evident in microregions such as Garanhuns, where a reduction in the frequency of atmospheric heat waves is observed (Table 5). However, a significant increase in the magnitude of coupled events is also observed (Table 7). This contrast indicates that, although less frequent, events in these areas are becoming more intense.

In general, the trends associated with land surface temperature confirm its greater sensitivity to environmental changes. Even in regions where air temperature did not show a significant trend, LST recorded a consistent increase in the frequency and duration of heat waves (Table 6). This result indicates that analyses based exclusively on air temperature may underestimate the intensification of thermal stress.

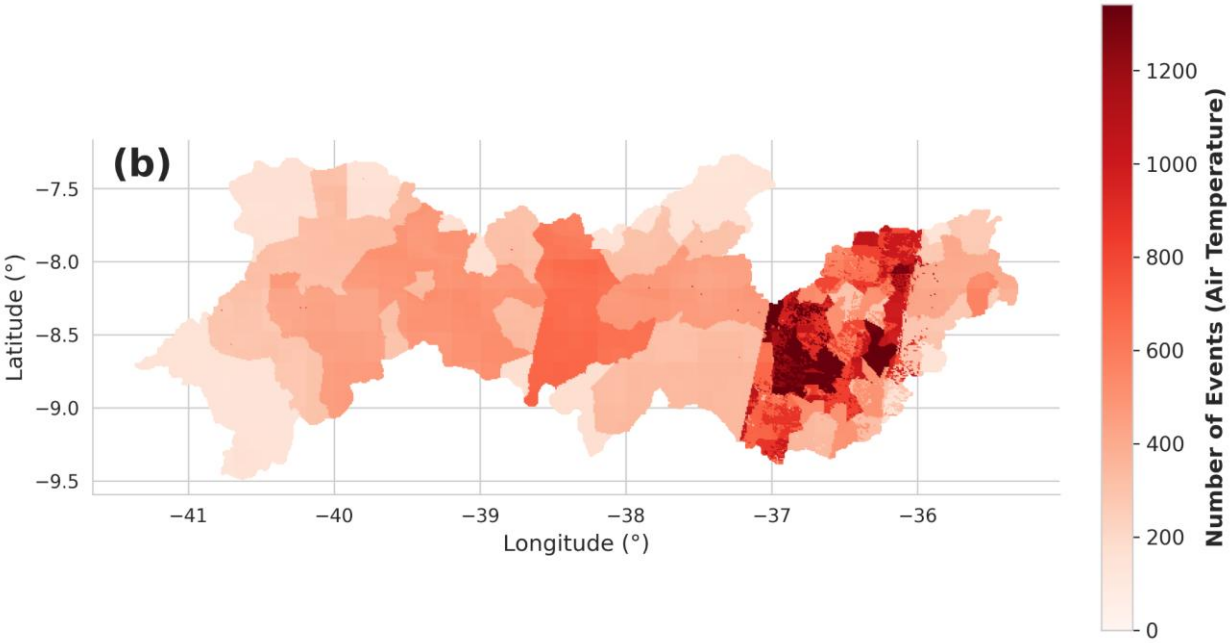
This divergence between LST and Tair agrees with studies showing the greater sensitivity of surface temperature to local conditions, including land cover and water availability (Zhang et al. 2024). In semiarid environments, the limitation of evapotranspiration favors the increase of the sensible heat flux, intensifying surface warming and amplifying thermal extremes (Miralles et al. 2014). As a result, LST is a more sensitive indicator of changes in the regional thermal regime.

3.7 Spatial patterns of vulnerability to heat waves

The spatial analysis revealed persistent patterns of thermal vulnerability in the Pernambuco Semiarid region (Fig. 6). The microregions of the Sertão do Pajeú and Sertão do Moxotó constitute the main hotspot of heat wave occurrence, both for LST and for coupled events.


(a)
Latitude (°)
−7.5
−8.0
−8.5
−9.0
−9.5
−41
−40
−39
−38
−37
−36
Longitude (°)
Number of Events (LST)
200
175
150
125
100
75
50
25
0

525


(b)
Latitude (°)
−7.5
−8.0
−8.5
−9.0
−9.5
−41
−40
−39
−38
−37
−36
Longitude (°)
Number of Events (Air Temperature)
1200
1000
800
600
400
200
0

526

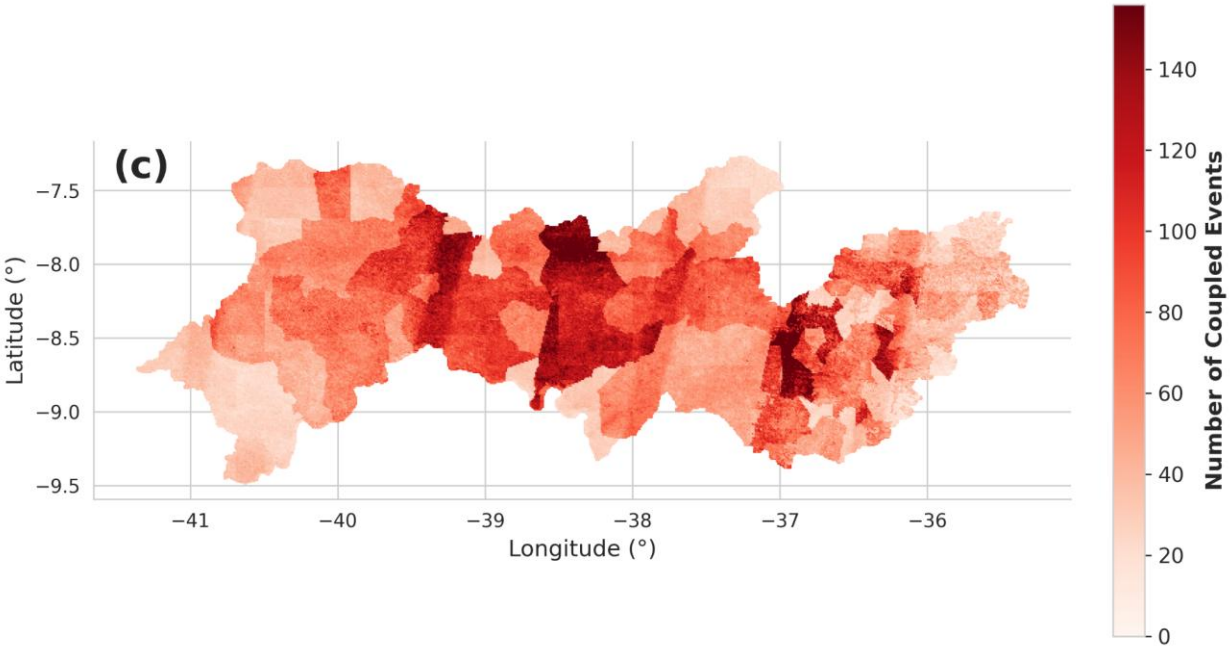


Fig. 6 Spatial distribution of the mean frequency of heat waves in the Pernambuco Semiarid region (1994–2023): (a) land surface temperature (LST); (b) air temperature (Tair); (c) coupled events (LST + Tair). The color scale ranges from white (low frequency) to dark red (high frequency)

These areas overlap with regions of high susceptibility to desertification, which is consistent with a link between land degradation and surface warming that this study did not test directly. By contrast, regions of the Agreste and areas close to the Zona da Mata present a lower frequency of events, consistent with the moderating effect of higher humidity and elevation. The comparison between LST and Tair shows the limitations of the reanalysis, which tends to homogenize the thermal risk, whereas LST reveals significant local heterogeneities.

3.8 Comparative characteristics of heat waves

The comparative analysis of the metrics (Table 8) indicates that surface heat waves are more persistent and energetic than atmospheric events. While Tair events have a mean duration of

6 days and low intensity (~0.7 °C), LST events reach a mean duration of 12 days and greater thermal magnitude.

Table 8 Comparative statistical summary of the heat wave metrics identified in the Pernambuco Semiarid region (1994–2023)

Event	Frequency	Duration (days)	Intensity (°C)	Magnitude (°C)
Heat Waves — Surface	55,758	12	2	27
Heat Waves — Atmosphere	93,602	6	0.7	5
Coupled Events	31,097	6	1.4	11

Note: Frequency refers to the sum of all occurrences of distinct clusters detected in the historical series. Duration is the mean number of days per event. Intensity represents the mean anomaly above the 90th percentile threshold. Magnitude corresponds to the accumulated thermal load (sum of the intensities over the duration of the event). For coupled events, the intensity and magnitude metrics are presented separately for the surface component (LST) and the atmospheric component (Air).

Coupled events exhibit an intermediate frequency but greater atmospheric intensity (~1.4 °C), although part of this difference is expected by construction, because requiring a simultaneous surface event selects the hottest days. This pattern is consistent with the role of the surface as a modulator and amplifier of thermal extremes in semiarid regions (Miralles et al. 2014; Hu et al. 2023).

4 Conclusions

The integration of atmospheric reanalysis (ERA5) and remote sensing data (Landsat) enabled consistent characterization of the spatio-temporal variability of heat waves in the Pernambuco Semiarid region from 1994 to 2023.

The results partially confirm the initial hypothesis. No significant trend was detected in atmospheric heat waves, which remain governed by natural climate variability. Surface heat waves, however, showed a robust and statistically significant increase in both frequency and duration. This contrast shows that the intensification of regional thermal stress is not adequately captured when assessments rely exclusively on air temperature.

In addition, coupled events (LST + Tair) increased significantly, particularly after 2013, which is consistent with a strengthening of soil–atmosphere feedback. This mechanism was not measured directly, and part of the post-2013 increase may reflect the denser Landsat sampling.

From a spatial perspective, warming does not occur homogeneously. The microregions of the Sertão, particularly Pajeú, Moxotó, Salgueiro, and Itaparica, concentrate the greatest increase in event frequency, while transition areas, such as Brejo Pernambucano and Garanhuns, show greater intensification of magnitude, indicating distinct patterns of thermal vulnerability.

The results also suggest that land surface temperature (LST) responds more strongly than air temperature to surface conditions, although part of its greater variability reflects the finer spatial resolution of Landsat. LST therefore complements analyses based on air temperature.

These findings reinforce the need for integrated approaches in climate monitoring, especially in semiarid regions, where surface degradation may contribute to the intensification of thermal extremes.

Statements and Declarations

Funding

This work was supported by the Fundação de Amparo à Ciência e Tecnologia do Estado de Pernambuco (FACEPE), Brazil, under Grant No. IBPG-0079-3.07/24.

Competing interests

The authors have no relevant financial or non-financial interests to disclose.

Author contributions

Isabela Patrícia de Andrade Figueira: conceptualization, methodology, software, data curation, formal analysis, investigation, visualization, writing – original draft. Aldo Torres Sales: conceptualization, supervision, methodology, validation, writing – review and editing. Alan Cezar Bezerra: methodology, validation, writing – review and editing. Alexandre Hugo Cezar Barros: validation, writing – review and editing. Jhon Lennon Bezerra da Silva: validation, writing – review and editing. Marcus Metri Corrêa: supervision, validation, writing – review and editing. All authors read and approved the final manuscript.

Data availability

The Landsat Collection 2 images (LANDSAT/LT05/C02/T1_TOA, LANDSAT/LC08/C02/T1_TOA and LANDSAT/LC09/C02/T1_TOA) and the ERA5 reanalysis are publicly available through the Google Earth Engine data catalog and the Copernicus Climate Data Store. INMET station records are publicly available from the INMET Meteorological Database for Teaching and Research (BDMEP).

Code availability

The Google Earth Engine and Python scripts used in this study are publicly available on GitHub at https://github.com/isabelaandrade-droid/Ondas_de_Calor-SemiaridoPE.

Ethics approval

Not applicable.

Consent to participate

Not applicable.

Consent for publication

Not applicable.

References

Agathangelidis I, Cartalis C, Polydoros A, et al (2022) Can satellite-based thermal anomalies be indicative of heat-waves? An investigation for MODIS land surface temperatures in the Mediterranean region. Remote Sens 14:3139. https://doi.org/10.3390/rs14133139

Almeida M, Coelho P (2023) A first assessment of ERA5 and ERA5-Land reanalysis air temperature in Portugal. Int J Climatol 43:6643–6663. https://doi.org/10.1002/joc.8225

Araújo CSP, Silva IAC, Ippolito M, Almeida CDGC (2022) Evaluation of air temperature estimated by ERA5-Land reanalysis using surface data in Pernambuco, Brazil. Environ Monit Assess 194:381. https://doi.org/10.1007/s10661-022-10047-2

Araújo CSP, Silva JRI, Almeida CDGC (2025) Total precipitation and air temperature data obtained from ERA5-Land reanalysis: validation and accuracy. Rev Caatinga 38:e12578. https://doi.org/10.1590/1983-21252025v3812578rc

618 Barbosa HA (2023) Flash drought and its characteristics in Northeastern South America during
619 2004–2022 using satellite-based products. Atmosphere 14:1629.
620 https://doi.org/10.3390/atmos14111629
621 Barbosa HA (2024) Understanding the rapid increase in drought stress and its connections with
622 climate desertification since the early 1990s over the Brazilian semi-arid region. J Arid
623 Environ 222:105142. https://doi.org/10.1016/j.jaridenv.2024.105142
624 Barbosa HA, Lakshmi Kumar TV, Silva LRM (2015) Recent trends in vegetation dynamics in
625 the South America and their relationship to rainfall. Nat Hazards 77:883–899.
626 https://doi.org/10.1007/s11069-015-1635-8
627 Barriopedro D, García-Herrera R, Ordóñez C, et al (2023) Heat waves: physical understanding
628 and scientific challenges. Rev Geophys 61:e2022RG000780.
629 https://doi.org/10.1029/2022RG000780
630 Bartusek S, Kornhuber K, Ting M (2022) 2021 North American heat-wave amplified by climate
631 change-driven nonlinear interactions. Nat Clim Change 12:1143–1150.
632 https://doi.org/10.1038/s41558-022-01520-4
633 Bell B, Hersbach H, Simmons A, et al (2021) The ERA5 global reanalysis: preliminary
634 extension to 1950. Q J R Meteorol Soc 147:4186–4227. https://doi.org/10.1002/qj.4174
635 Bezerra DF, da Silva Júnior JC, Gonçalves GE, de Medeiros VWC (2019) Availability analysis
636 of the Brazilian's national weather measurement system. Rev Bras Comput Apl 11:146–154.
637 https://doi.org/10.5335/rbca.v11i3.10026
638 Bindajam AA, Mallick J, Hang HT, et al (2020) Impacts of vegetation and topography on land
639 surface temperature variability over the semi-arid mountain cities of Saudi Arabia.
640 Atmosphere 11:762. https://doi.org/10.3390/atmos11070762

Carrión D, Arfer KB, Rush J, et al (2021) A 1-km hourly air-temperature model for 13 northeastern U.S. states using remotely sensed and ground-based measurements. Environ Res 200:111477. https://doi.org/10.1016/j.envres.2021.111477

CEMADEN (2018) Technical report: the multiyear 2012–2017 drought in the Northeast. Centro Nacional de Monitoramento e Alertas de Desastres Naturais, São José dos Campos

Chang KL, Schultz MG, Lan X, et al (2021) Trend detection of atmospheric time series: incorporating appropriate uncertainty estimates and handling extreme events. Elementa: Science of the Anthropocene 9:00035. https://doi.org/10.1525/elementa.2021.00035

Chen L, Brun P, Buri P, et al (2025) Global increase in the occurrence and impact of multiyear droughts. Science 387:278–284. https://doi.org/10.1126/science.ado4245

Chen X, Guo Z, Chen J, et al (2019) Replacing the red band with the red-SWIR band (0.74ρred+0.26ρswir) can reduce the sensitivity of vegetation indices to soil background. Remote Sens 11:851. https://doi.org/10.3390/rs11070851

Cohen I, Zandalinas SI, Huck C, et al (2020) Meta-analysis of drought and heat stress combination impact on crop yield and yield components. Physiol Plant 171:66–76. https://doi.org/10.1111/ppl.13203

Crawford CJ, Roy DP, Arab S, et al (2023) The 50-year Landsat collection 2 archive. Sci Remote Sens 8:100103. https://doi.org/10.1016/j.srs.2023.100103

Dumitrescu A, Brabec M, Cheval S (2020) Statistical gap-filling of SEVIRI land surface temperature. Remote Sens 12:1423. https://doi.org/10.3390/rs12091423

Duveiller G, Hooker J, Cescatti A (2018) The mark of vegetation change on Earth's surface energy balance. Nat Commun 9:679. https://doi.org/10.1038/s41467-017-02810-8

663 Ermida SL, Soares P, Mantas V, et al (2020) Google Earth Engine open-source code for land
664 surface temperature estimation from the Landsat series. Remote Sens 12:1471.
665 https://doi.org/10.3390/rs12091471
666 Faybishenko B, Versteeg R, Pastorello G, et al (2021) Challenging problems of quality assurance
667 and quality control (QA/QC) of meteorological time series data. Stoch Environ Res Risk
668 Assess 36:1049–1062. https://doi.org/10.1007/s00477-021-02106-w
669 Gorelick N, Hancher M, Dixon M, et al (2017) Google Earth Engine: planetary-scale geospatial
670 analysis for everyone. Remote Sens Environ 202:18–27.
671 https://doi.org/10.1016/j.rse.2017.06.031
672 Hersbach H, Bell B, Berrisford P, et al (2020) The ERA5 global reanalysis. Q J R Meteorol Soc
673 146:1999–2049. https://doi.org/10.1002/qj.3803
674 Holmes TRH, Hain CR, Anderson MC, Crow WT (2016) Cloud tolerance of remote-sensing
675 technologies to measure land surface temperature. Hydrol Earth Syst Sci 20:3263–3275.
676 https://doi.org/10.5194/hess-20-3263-2016
677 Hu Y, Jia G, Gao H, et al (2023) Spatial characterization of global heat waves using satellite-
678 based land surface temperature. Int J Appl Earth Obs Geoinf 125:103604.
679 https://doi.org/10.1016/j.jag.2023.103604
680 IBGE (2017) Malha municipal 2017. Instituto Brasileiro de Geografia e Estatística, Rio de
681 Janeiro. https://www.ibge.gov.br/geociencias/organizacao-do-territorio/malhas-
682 territoriais/15774-malhas.html. Accessed 29 Oct 2026
683 IPCC (2023) Climate change 2023: synthesis report. Contribution of Working Groups I, II and
684 III to the Sixth Assessment Report of the Intergovernmental Panel on Climate Change. IPCC,
685 Geneva. https://doi.org/10.59327/IPCC/AR6-9789291691647

686 Jardim AMRF, Araújo Júnior GN, Silva MV, et al (2022) Using remote sensing to quantify the
687 joint effects of climate and land use/land cover changes on the Caatinga biome of Northeast
688 Brazilian. Remote Sens 14:1911. https://doi.org/10.3390/rs14081911
689 Jiménez-Esteve B, Domeisen DIV (2022) The role of atmospheric dynamics and large-scale
690 topography in driving heat-waves. Q J R Meteorol Soc 148:2344–2367.
691 https://doi.org/10.1002/qj.4306
692 Karinou F, Agathangelidis I, Cartalis C (2025) Assessing the combined impact of land surface
693 temperature and droughts to heat-waves over Europe between 2003 and 2023. Remote Sens
694 17:1655. https://doi.org/10.3390/rs17091655
695 Kodimalar T, Vidhya R, Eswar R (2020) Land surface emissivity retrieval from multiple
696 vegetation indices: a comparative study over India. Remote Sens Lett 11:176–185.
697 https://doi.org/10.1080/2150704X.2019.1692384
698 Liu HQ, Huete A (1995) A feedback based modification of the NDVI to minimize canopy
699 background and atmospheric noise. IEEE Trans Geosci Remote Sens 33:457–465.
700 https://doi.org/10.1109/36.377946
701 Liu H, Lu N, Jiang H, et al (2020) Filling gaps of monthly Terra/MODIS daytime land surface
702 temperature using discrete cosine transform method. Remote Sens 12:361.
703 https://doi.org/10.3390/rs12030361
704 Marengo JA, Cunha APMA, Nobre CA, et al (2020) Assessing drought in the drylands of
705 northeast Brazil under regional warming exceeding 4 °C. Nat Hazards 103:2589–2611.
706 https://doi.org/10.1007/s11069-020-04097-3

Marengo JA, Costa MC, Cunha AP, et al (2026) Characterisation of the exceptional heat-wave conditions observed in Brazil during the record-hot years of 2024 and 2025. Int J Climatol 46:e70219. https://doi.org/10.1002/joc.70219

Martins KBS, Souto PC, Souto JS, et al (2025) Reflectância, variação da temperatura e conteúdo de água do solo em caatinga degradada na Paraíba. Rev Bras Sensoriamento Remoto 5(2). https://doi.org/10.5281/zenodo.14613195

Miralles DG, Teuling AJ, van Heerwaarden CC, Vilà-Guerau de Arellano J (2014) Mega-heatwave temperatures due to combined soil desiccation and atmospheric heat accumulation. Nat Geosci 7:345–349. https://doi.org/10.1038/ngeo2141

Miralles DG, Gentine P, Seneviratne SI, Teuling AJ (2019) Land–atmospheric feedbacks during droughts and heat-waves: state of the science and current challenges. Ann N Y Acad Sci 1436:19–35. https://doi.org/10.1111/nyas.13912

Mo Y, Xu Y, Chen H, Zhu S (2021) A review of reconstructing remotely sensed land surface temperature under cloudy conditions. Remote Sens 13:2838. https://doi.org/10.3390/rs13142838

Mora C, Spirandelli D, Franklin EC, et al (2018) Broad threat to humanity from cumulative climate hazards intensified by greenhouse gas emissions. Nat Clim Change 8:1062–1071. https://doi.org/10.1038/s41558-018-0315-6

NPant KK, Naik J, Barthakur S, Chandra V (2025) High-temperature stress in wheat (Triticum aestivum L.): unfolding the impacts, tolerance and methods to mitigate the detrimental effects. Cereal Res Commun 53:1171–1197. https://doi.org/10.1007/s42976-025-00634-7

Perkins SE, Alexander LV (2013) On the measurement of heat waves. J Clim 26:4500–4517. https://doi.org/10.1175/JCLI-D-12-00383.1

730 Perkins-Kirkpatrick SE, Lewis SC (2020) Increasing trends in regional heat-waves. Nat
731 Commun 11:3357. https://doi.org/10.1038/s41467-020-16970-7
732 Reis NCS, Boiaski NT, Ferraz SET (2019) Characterization and spatial coverage of heat waves
733 in subtropical Brazil. Atmosphere 10:284. https://doi.org/10.3390/atmos10050284
734 Roffe SJ, van der Walt AJ (2023) Representation and evaluation of southern Africa's seasonal
735 mean and extreme temperatures in the ERA5-based reanalysis products. Atmos Res
736 284:106591. https://doi.org/10.1016/j.atmosres.2022.106591
737 Schween JH, Hoffmeister D, Löhnert U (2020) Filling the observational gap in the Atacama
738 Desert with a new network of climate stations. Glob Planet Change 184:103034.
739 https://doi.org/10.1016/j.gloplacha.2019.103034
740 Seneviratne SI, Corti T, Davin EL, et al (2010) Investigating soil moisture–climate interactions
741 in a changing climate: a review. Earth-Sci Rev 99:125–161.
742 https://doi.org/10.1016/j.earscirev.2010.02.004
743 Shiff S, Helman D, Lensky IM (2021) Worldwide continuous gap-filled MODIS land surface
744 temperature dataset. Sci Data 8:74. https://doi.org/10.1038/s41597-021-00861-7
745 Silva AL, Sheridan S, Ibebuchi C, Lee C (2025) Comparing observed and reanalysis data for
746 trends in extreme temperature events in Brazil (1996–2022). Theor Appl Climatol 156:546.
747 https://doi.org/10.1007/s00704-025-05777-5
748 SUDENE (2017) Resolução nº 107, de 27 de julho de 2017. Conselho Deliberativo da
749 Superintendência do Desenvolvimento do Nordeste, Recife
750 Tamiminia H, Salehi B, Mahdianpari M, et al (2020) Google Earth Engine for geo-big data
751 applications: a meta-analysis and systematic review. ISPRS J Photogramm Remote Sens
752 164:152–170. https://doi.org/10.1016/j.isprsjprs.2020.04.001

USGS (2022) USGS opens door to Landsat 9 data. U.S. Geological Survey. https://www.usgs.gov/news/technical-announcement/usgs-opens-door-landsat-9-data. Accessed 11 Feb 2026

Velikou K, Lazoglou G, Tolika K, Anagnostopoulou C (2022) Reliability of the ERA5 in replicating mean and extreme temperatures across Europe. Water 14:543. https://doi.org/10.3390/w14040543

Vicente-Serrano SM, Peña-Angulo D, Beguería S, et al (2022) Global drought trends and future projections. Philos Trans R Soc A 380:20210285. https://doi.org/10.1098/rsta.2021.0285

Wijedasa LS, Sloan S, Michelakis DG, Clements GR (2012) Overcoming limitations with Landsat imagery for mapping of peat swamp forests in Sundaland. Remote Sens 4:2595–2618. https://doi.org/10.3390/rs4092595

Wu CY, Mossa J, Mao L, Almulla M (2019) Comparison of different spatial interpolation methods for historical hydrographic data of the lowermost Mississippi River. Ann GIS 25:133–151. https://doi.org/10.1080/19475683.2019.1588781

Wu Q (2020) geemap: a Python package for interactive mapping with Google Earth Engine. J Open Source Softw 5:2305. https://doi.org/10.21105/joss.02305

Wulder MA, White JC, Masek JG, et al (2011) Continuity of Landsat observations: short term considerations. Remote Sens Environ 115:747–751. https://doi.org/10.1016/j.rse.2010.11.002

Xu W, Lei X, Chen S, et al (2022) How well does the ERA5 reanalysis capture the extreme climate events over China? Part II: extreme temperature. Front Environ Sci 10:921659. https://doi.org/10.3389/fenvs.2022.921659

774 Yu Y, Xiao W, Zhang Z, et al (2021) Evaluation of 2-m air temperature and surface temperature
775 from ERA5 and ERA-I using buoy observations in the Arctic during 2010–2020. Remote
776 Sens 13:2813. https://doi.org/10.3390/rs13142813
777 Zeng X, Hui Y, Shen J, et al (2023) An empirical evaluation of columnar storage formats.
778 arXiv:2304.05028. https://doi.org/10.48550/arXiv.2304.05028
779 Zhang J, Guan Q, Zhang Z, et al (2024) Characteristics of spatial and temporal dynamics of
780 vegetation and its response to climate extremes in ecologically fragile and climate change
781 sensitive areas – a case study of Hexi region. Catena 239:107910.
782 https://doi.org/10.1016/j.catena.2024.107910